NeuroImage xxx (2012) xxx–xxx

Contents lists available at SciVerse ScienceDirect

NeuroImage

journal homepage: www.elsevier.com/locate/ynimg

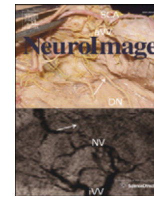

Cortical thickness and central surface estimation

Robert Dahnke *, Rachel Aine Yotter [1], Christian Gaser [1]

Department of Psychiatry, University of Jena, Jahnstrasse 3, D-07743 Jena, Germany

ARTICLE INFO

Article history:
Accepted 20 September 2012
Available online xxxx

Keywords:
MRI
Cortical thickness
Central surface
Surface reconstruction
Brain
Phantom
Validation

ABSTRACT

Several properties of the human brain cortex, e.g., cortical thickness and gyrification, have been found to correlate with the progress of neuropsychiatric disorders. The relationship between brain structure and function harbors a broad range of potential uses, particularly in clinical contexts, provided that robust methods for the extraction of suitable representations of the brain cortex from neuroimaging data are available. One such representation is the computationally defined central surface (CS) of the brain cortex. Previous approaches to semi-automated reconstruction of this surface relied on image segmentation procedures that required manual interaction, thereby rendering them error-prone and complicating the analysis of brains that were not from healthy human adults. Validation of these approaches and thickness measures is often done only for simple artificial phantoms that cover just a few standard cases. Here, we present a new fully automated method that allows for measurement of cortical thickness and reconstructions of the CS in one step. It uses a tissue segmentation to estimate the WM distance, then projects the local maxima (which is equal to the cortical thickness) to other GM voxels by using a neighbor relationship described by the WM distance. This projection-based thickness (PBT) allows the handling of partial volume information, sulcal blurring, and sulcal asymmetries without explicit sulcus reconstruction via skeleton or thinning methods. Furthermore, we introduce a validation framework using spherical and brain phantoms that confirms accurate CS construction and cortical thickness measurement under a wide set of parameters for several thickness levels. The results indicate that both the quality and computational cost of our method are comparable, and may be superior in certain respects, to existing approaches.

Introduction

The cerebral cortex is a highly folded sheet of gray matter (GM) that lies inside the cerebrospinal fluid (CSF) and surrounds a core of white matter (WM). Besides the separation into two hemispheres, the cortex is macroscopically structured into outwardly folded gyri and inwardly folded sulci (Fig. 1). The cortex can be described by the outer surface (or boundary) between GM and CSF, the inner surface (or boundary) between GM and WM, and the central surface (CS) (Fig. 1). Cortical structure and thickness were found to be an important biomarker for normal development and aging (Fjell et al., 2006; Sowell et al., 2004, 2007) and pathological changes (Kuperberg et al., 2003; Rosas et al., 2008; Sailer et al., 2003; Thompson et al., 2004) in not only humans, but also other mammals (Hofman, 1989; Zhang and Sejnowski, 2000).

Although MR images allow in vivo measurements of the human brain, data is often limited by its sampling resolution that is usually around 1 mm^3. At this resolution, the CSF is often hard to detect in sulcal areas due to the partial volume effect (PVE). The PVE comes into effect for voxels that contain more than one tissue type and have an intensity gradient that lies somewhere between that of the pure tissue classes. Normally, the PVE describes the boundary with a sub-voxel accuracy, but within a sulcus the CSF volume is small and affected by noise, rendering it difficult to describe the outer boundary in this region (blurred sulcus, Fig. 2). Thus, to obtain an accurate thickness measurement, an explicit reconstruction of the outer boundary based on the inner boundary is necessary. This can be done by skeleton (or thinning) methods or alternatively by model-based deformation of the inner surface. Skeleton-based reconstruction of the outer boundary is used by CLASP (Kim et al., 2005; Lee et al., 2006a,2006b; Lerch and Evans, 2005), CRUISE (Han et al., 2004; Tosun et al., 2004; Xu et al., 1999), Caret (Van Essen et al., 2001), the Laplacian approach (Acosta et al., 2009; Haidar and Soul, 2006; Hutton et al., 2008; Jones et al., 2000; Rocha et al., 2007; Yezzi and Prince, 2003), and other volumetric methods (Eskildsen and Ostergaard, 2006, 2007; Hutton et al., 2008; Lohmann et al., 2003). Methods without sulcal modeling will tend to overestimate thickness in blurred regions (Jones et al., 2000; Lohmann et al., 2003) or must concentrate exclusively on non-blurred gyral regions (Sowell et al., 2004). Alternatively, cortical thickness may be estimated via deformation of the inner surface (FreeSurfer (Dale et al., 1999; Fischl and Dale, 2000), DiReCT (Das et al., 2009), Brainvoyager (Kriegeskorte and Goebel, 2001), Brainsuite (Shattuck and Leahy, 2001; Zeng et al., 1999) or coupled surfaces (ASP (Kabani et al., 2001; MacDonald et al., 2000). Considering that the accuracy of

* Corresponding author. Fax: +49 3641 934755.
E-mail addresses: robert.dahnke@uni-jena.de (R. Dahnke), rachel.yotter@uni-jena.de (R.A. Yotter), christian.gaser@uni-jena.de (C. Gaser).
[1] Fax: +49 3641 934755.

1053-8119/$ – see front matter © 2012 Published by Elsevier Inc.
http://dx.doi.org/10.1016/j.neuroimage.2012.09.050

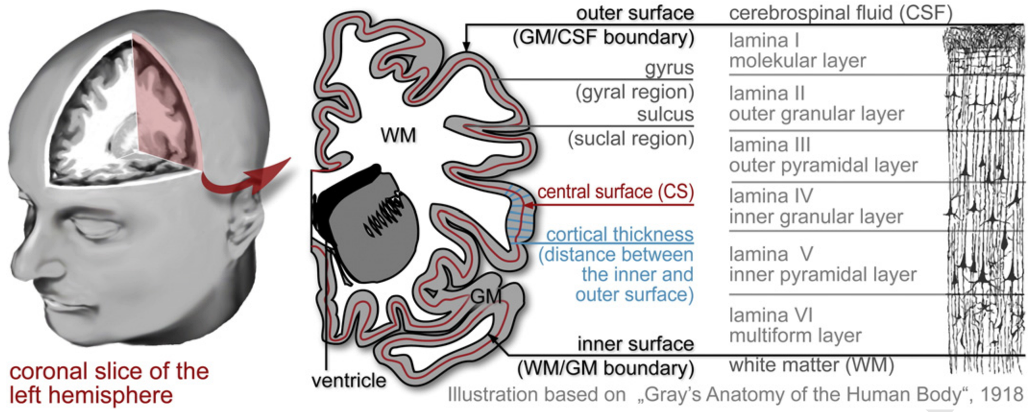

Fig. 1. The cortex: Shown is an illustration of the cortical macro- and microstructure. The cerebral cortex is a highly folded sheet of gray matter (GM) that lies inside the cerebrospinal fluid (CSF) and surrounds a core of white matter (WM). Inwardly folded regions are called sulci whereas outwardly folded areas are denoted as gyri. There are three common surfaces to describe this sheet: the outer surface, the inner surface, and the central surface (CS). The CS allows a better representation of the cortical GM sheet and improved accuracy of cortical surface measurements. Cortical thickness describes the distance between the inner surface and the outer surface and is related to cortical development and diseases such as Alzheimer's.

the measurement depends strongly upon the precision of cortical surface reconstruction at the inner and outer boundaries, and that the computation time is often related to the anatomical accuracy of the reconstruction, such measurements may require intensive computational resources in order to achieve the final measurement.

Here, we present a new volume-based algorithm, PBT (Projection Based Thickness), that uses a projection scheme which considers blurred sulci to create a correct cortical thickness map. For validation, we compare PBT to the volumetric Laplacian approach and the surface-based approach included in the FreeSurfer (v 4.5) software package. If the results from PBT are approximately the same as that achieved by FreeSurfer and a significant improvement over the Laplacian approach, it may be concluded that PBT is a highly accurate volume-based method for measuring cortical thickness. For situations in which extensive surface analysis is not required, PBT would allow the exclusion of cortical surface reconstruction steps with no loss of accuracy for cortical thickness measurements.

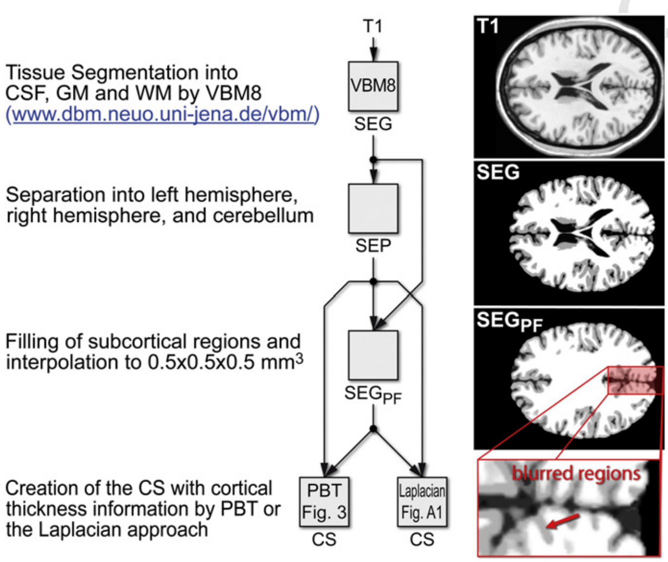

Fig. 2. Main flow diagram: Shown is a flow diagram of the pre-processing steps of the CS and thickness estimation. A tissue segmentation algorithm (from VBM8) is used to create a segmentation image SEG from an anatomical image. This segmentation image is used for (manual) separation of the cortex into two hemispheres and removal of the cerebellum with hindbrain, resulting in a map SEP. This map creates the map SEG_{PF}, a masked version of SEG with filled ventricular and subcortical regions. Both approaches used an interpolated version of the map SEG_{PF} to create a CS with a cortical thickness value of each vertex. The red subfigure shows blurred sulcal regions, where CSF voxels were detected as GM due to noise removal included in the segmentation algorithm. These blurred regions need an explicit reconstruction of the outer surface for the Laplacian approach (Fig. 4), whereas PBT uses an inherent scheme to account for these regions (Fig. 3). (For interpretation of the references to color in this figure legend, the reader is referred to the web version of this article.)

We also propose a suite of test cases using a variety of phantoms with different parameters as a suggestion for how a cortical thickness measurement approach could be rigorously tested for validity and stability. Previously published validation approaches that used a spherical phantom (Acosta et al., 2009; Das et al., 2009) often addressed only one thickness and curvature (radii) of the inner and outer boundary. The problem is that the measure may work well for this special combination of parameters, but performance can change for different radii. Another limitation is that this phantom describes only areas where the CSF intensity is high enough, but most sulcal areas (that comprise over half of the human cortex) are blurred. Our test suite directly addresses these concerns.

The cortical thickness map may also be subsequently used to generate a reconstruction of the CS. Compared to the inner or outer surface, the CS allows a better representation of the cortical sheet (Van Essen et al., 2001), since neither sulcal or gyral regions are over- or underestimated (Scott and Thacker, 2005). As the average of two boundaries, it is less error-prone to noise and it allows a better mapping of volumetric data (Liu et al., 2008; Van Essen et al., 2001). Generally, a surface reconstruction allows surface-based analysis that is not restricted to the grid and allows metrics, such as the gyrification index (Schaer et al., 2008) or other convolution measurements (Luders et al., 2006; Mietchen and Gaser, 2009; Rodriguez-Carranza et al., 2008; Toro et al., 2008), that can only be measured using surface meshes (Dale et al., 1999). It provides surface-based smoothing that gives results superior to that obtained from volumetric smoothing (Lerch and Evans, 2005). Furthermore, surface meshes allow a better visualization of structural and functional data, especially when they are inflated (Fischl et al., 1999) or flattened (Van Essen and Drury, 1997). Due to these considerations, we have explored the quality of the cortical surface reconstructions.

Material and methods

We start with a short overview about the main steps of our method and the Laplacian approach; algorithmic details are separately described in the following subchapters.

MRI images are first segmented into different tissue classes using VBM8[2](Fig. 2; see Segmentation). This segmentation is used for (manual) separation of the hemispheres and removal of the cerebellum with hindbrain, resulting in a map SEP. This map creates the map SEG_{PF}, a masked version of SEG with filled ventricular and subcortical regions. To take into account the small sulci with thicknesses of around 1 mm, SEG_{PF} was linearly interpolated to $0.5\times0.5\times0.5$ mm^3 (Hutton et al., 2008; Jones et al., 2000).

For each GM voxel, the distance from the inner boundary was estimated within the GM using a voxel-based distance method (see Distance measure). The result is a WM distance map WMD, whose values at the outer GM boundary represent the GM thickness. These values at the outer boundary were then projected back to the inner boundary, resulting in a GM thickness map GMT. The relation between the WMD and GMT maps creates the percentage position map PP that is used to create the CS at the 50% level (see Projection-based thickness).

As a basis of comparison, we constructed another CS using the Laplacian-based thickness measure (Jones et al., 2000) on the filled tissue segmentation map to create another set of GMT and PP maps. This method requires an explicit sulcal reconstruction step (Bouix and Kaleem, 2000) (see Laplacian-based thickness).

A topology correction based on spherical harmonics was used to correct the topology of the surfaces generated with the PBT and the Laplacian approach (Yotter et al., in press).

For validation, a set of spherical (SP; see Spherical phantoms) and brain phantoms (BP; see Brain phantoms) with uniform thickness were used to simulate different curvature, thickness, noise, and resolution levels. Since thickness and the location of the cortical surfaces were known, the two data sets could be directly compared. For thickness RMS error, the measured thickness was reduced by the expected thickness.

In addition to the spherical phantoms with equal thickness, we used the Collins brain phantom with different noise levels[3](Collins et al., 1998) and a real data set of 12 scans of the same subject of our database (see Real data) to compare our results to FreeSurfer 4.5. Because the real thickness of both data sets is unknown, we compare the results of each tested surface to the results of a surface that was generated on an averaged scan. RMS error was calculated for all vertices of a surface, including vertices of the filled subcortical regions and the corpus callosum. For these data sets, we evaluated the number of topological errors using Caret. To count the number of defects, the uncorrected CS was used for PBT and Laplacian, whereas for FreeSurfer the uncorrected WM surface was used. The CS of FreeSurfer was generated via Caret, where the positions of CS vertices were given by the mean positions of corresponding vertices of the inner and outer surface. Thickness RMS error was estimated based on the original FreeSurfer thickness results.

Segmentation

To achieve exact and stable results for thickness measures, the segmentation plays an important role. In principle, any segmentation for GM, WM, and CSF can be used. The segmentation could be binary maps, but to achieve more stable and exact results, it is important to use probability maps that are able to describe the boundary positions with sub-voxel accuracy (Hutton et al., 2008). Furthermore, inclusion of an additional noise removal step increases the accuracy and stability of the thickness measurements (Coupe et al., 2008). We used the VBM8 [4]toolbox (revision 388) for SPM8[5](Ashburner and Friston, 2005) (revision 4290) for segmentation of all T1 images, which includes an optimized Rician non-local mean (ORNLM) (Coupe et al., 2008) and a Gaussian Hidden Markov Random Field (GHMRF) (Cuadra et al., 2005) filter for noise reduction (NR). The probability tissue maps CSF, GM, and WM are combined in one probability image SEG (Tohka et al., 2004). Pure tissue voxels are coded with integers (background = 0, CSF = 1, GM = 2, WM = 3), whereas values between integers describe the percentile relation between the tissues. For example, a voxel with an intensity of 2.56 contains 44% GM and 56% WM and a value of 1.92 contains 92% GM and 8% CSF. Hence, tissue boundaries are at 0.5 between background and CSF, 1.5 between CSF and GM and 2.5 between GM and WM. Note that this map is only able to describe two tissue classes per voxel. However, this does not degrade our analyses, because most anatomical images do not provide more information for the segmentation. Furthermore, most regions with no GM layer, such as the brainstem or the near the ventricles, are cut or filled and thus are not included in the analysis.

Distance measure

To take into account the asymmetrical structures, we used the Eikonal equation with a non-uniform speed function $F(x)$ to find the closest boundary voxel $B(x)$ of a GM voxel x without passing a different boundary. To allow sub-voxel accuracy, the normalized vector between $B(x)$ and x is used to find a point $G(x)$ between x and $B(x)$. The intensity gradient between $B(x)$ and $G(x)$ allows a precise estimation of the boundary point $P(x)$, which is used to estimate the distance of x to the boundary.

In a more formal way, we solved the following Eikonal equation:

$$\begin{aligned} &F(x)\left\|\nabla D_{\mathrm{Ei}}(x)\right\| = 1, \quad for \quad x\in\Omega, \\ &D_{\mathrm{Ei}}(x) = 0, \quad for \quad x\in\Gamma, \end{aligned} \tag{1}$$

where x is a voxel, Ω is given by the GM, Γ is the object (the WM or the CSF and background), D_{Ei} is the Eikonal distance map, and $F(x)$ is the non-uniform speed map ($F_{\mathrm{WM}}(x)$ for the WM distance and $F_{\mathrm{CSF}}(x)$ for the CSF distance) that is given by the image intensity of SEG_{PF}:

$$\begin{aligned} F_{WM}(x) &= \min(1, \max(0, SEG_{PF}(x)-1)), \\ F_{CSF}(x) &= \min(1, \max(0, 3-SEG_{PF}(x))). \end{aligned} \tag{2}$$

In GM areas, $F_{\mathrm{WM}}(x)$ has a high "speed" which results in shorter distances, whereas in CSF areas the "speed" is very low and thus results in longer distances, whereas $F_{\mathrm{CSF}}(x)$ allows high speeds in GM and CSF areas, but not in WM regions. Because the distance map D_{Ei} contains distortions, it is only used to find the closest object voxel for each GM voxel $x\in\Omega$:

$$B_{Ei}(x, \Omega, \Gamma, F), \tag{3}$$

and to calculate the Euclidean distance D_{Eu} between the GM voxel x and its nearest WM voxel $B_{\mathrm{Ei}}(x, \Omega, \Gamma, F)$:

$$D_{Eu}(x, \Omega, \Gamma, F) = \left\|x, B_{Ei}(x, \Omega, \Gamma, F)\right\|_2. \tag{4}$$

We solve the above equations as follows: By solving the Eikonal equation within Ω, we also note the closest WM voxel B_{Ei}. To allow sub-voxel accuracy, the normalized vector between x and $B_{\mathrm{Ei}}(x, \Omega, \Gamma, F)$ is used to estimate a point $G(B_{\mathrm{Ei}}(x, \Omega, \Gamma, F))$ within one voxel distance to $B_{\mathrm{Ei}}(x, \Omega, \Gamma, F)$. The intensity gradient between $B_{\mathrm{Ei}}(x, \Omega, \Gamma, F)$ and $G(B_{\mathrm{Ei}}(x, \Omega, \Gamma, F))$ can then be used to estimate the exact boundary of Γ.

Projection-based thickness

For simplification we will use the terms of the GM, WM, and CSF probability maps for the operations, even though only the map SEG_{PF} is used. Cortical thickness can be described as the sum of the inner (WMD, Fig. 3b2) and outer (CSFD, Fig. 3b3) boundary distance.

[2] http://dbm.neuro.uni-jena.de/vbm/
[3] http://mouldy.bic.mni.mcgill.ca/brainweb/
[4] http://dbm.neuro.uni-jena.de/vbm/
[5] http://www.fil.ion.ucl.ac.uk/spm/

Please cite this article as: Dahnke, R., et al., Cortical thickness and central surface estimation, NeuroImage (2012), http://dx.doi.org/10.1016/j.neuroimage.2012.09.050

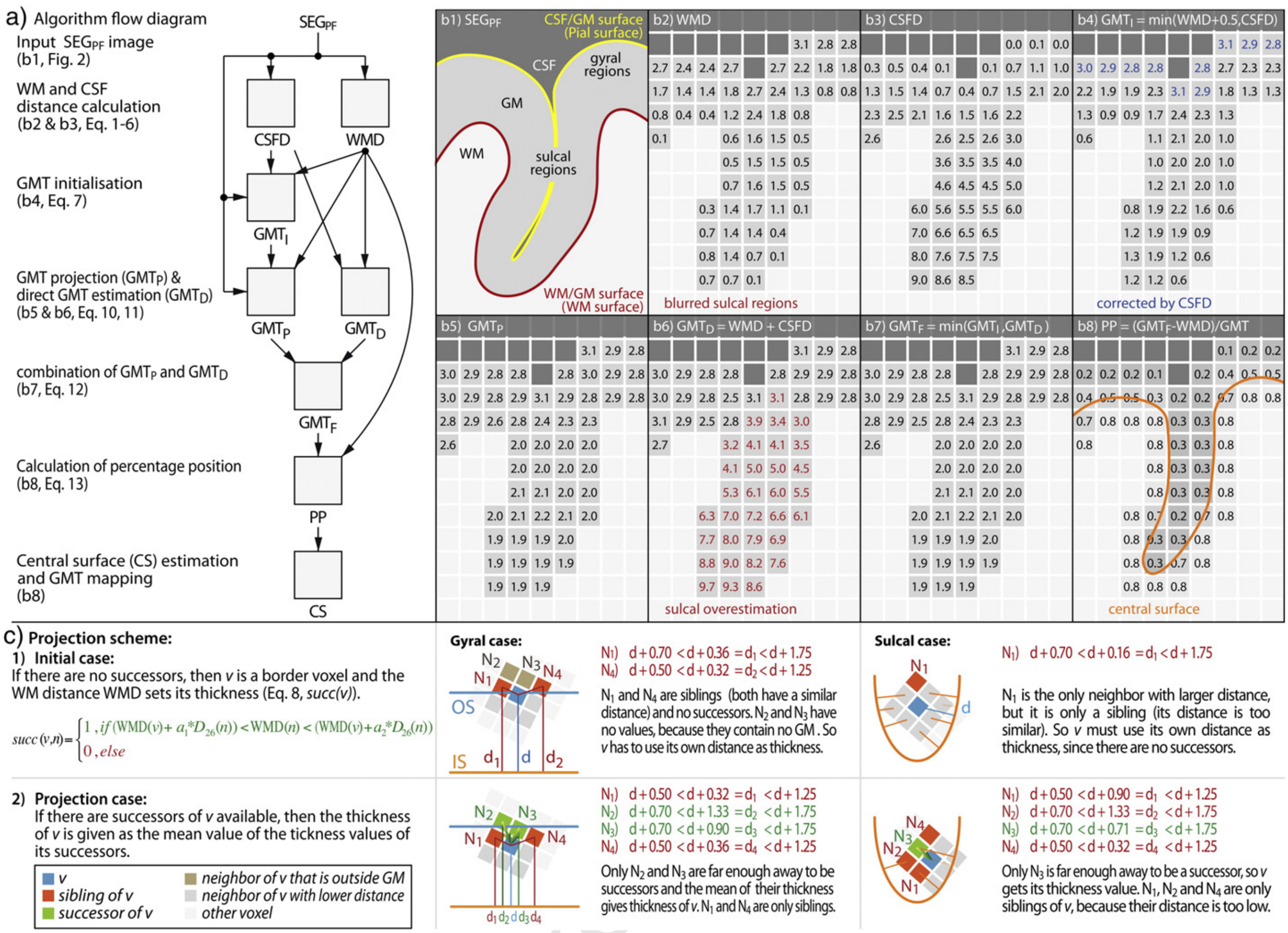

Fig. 3. PBT: Subfigure (a) shows a flow diagram of the PBT approach, whereas subfigure (b1–b8 with simplified titles) shows 2D illustrations of the volume maps of (a). In subfigure (c), we illustrate the most relevant cases of our PBT method — a gyral and a blurred sulcal case with initialization and projection step. For distance calculations, the Eikonal equation is solved to account for partial volume information. PBT starts with the (interpolated) masked segmentation image SEG$_{PF}$ shown in Fig. 2 and estimates the distance to the inner (b2) and outer (b3) boundary. The blurring of outer boundary in sulcal regions leads to strong overestimation of the real distance and finally to an overestimation of the cortical thickness. To get the correct values in these regions, PBT uses a modified version GMT$_I$ (b4) of the WMD, in which the local maximum describes the position of the outer boundary and the correct thickness. It now uses the successor relation *succ*(v) of a voxel v (Eq. (8)), given by the WM distance WMD (b2), to project thickness values from the outer boundary (b4) over the whole GM (b5). PBT additionally uses the direct GM thickness GMT$_D$ (b6) – which is overestimated in blurred areas, but helps to reduce artifacts such as blood vessels – to create a final map GMT$_F$ (b7) of the minimum thickness from both thickness maps. After estimation of cortical thickness, a percentage position map PP is generated to create the CS and map cortical thickness onto it. The projection scheme shown in subfigure (c) uses the WM distance map to project the maximum local WM distance that is equivalent to the local thickness to other voxels. The WM distance map allows the definition of successors (neighbors of a voxel v with a slightly larger distance than v) and siblings (neighboring voxel with a similar distance to v), and a voxel v gets the mean thickness of its successors. If a voxel has no successors, then it is located at the outer boundary and its WM distance is related to its size.

Blurring of the outer boundary in sulcal regions due to the PVE leads to an overestimation of the CSFD. To avoid the explicit reconstruction of the outer boundary by a skeleton, we focus on the information given by the WMD. At the outer boundary, and also within blurred regions, the GMT is fully described by the WMD, because the CSFD is zero (Lohmann et al., 2003; Sowell et al., 2004). In other words, the highest local WMD within the GM is identical to the GMT of this area, and it is only necessary to project this information to other GM voxels.

This can be done using the successor relationship of the WMD. A neighbor voxel v_2 of a voxel v_1 is a successor of v_1, if the WMD of v_2 is around one voxel greater than the WMD of v_1. Similarly, if the WMD of v_2 is around one voxel smaller than v_1, v_2 is labeled as the parent voxel. In this case, v_1 gets the thickness value of v_2. Neighbor voxels with a WMD similar to v_1 that are too close to be either a parent or a successor are called siblings, and their thicknesses remain unrelated to v_1. If v_1 has no successor, then it is a local maximum that is located at the CSF boundary and its GMT is given by its WMD.

We now want to describe this process in a more formal way, starting with the WMD:

$$WMD(v) = \begin{cases} D_{Eu}(v, GM > 0, WM, F_{WM}) & , if \;\; GM(v) > 0 \\ 0 & , otherwise \end{cases}, \tag{5}$$

where D_{Eu} gives the Euclidean distance of a voxel v to the nearest WM boundary that was found by solving the Eikonal equation for the speed map F_{WM} (Eq. (2)). The distance to the CSF boundary is now given by:

$$CSFD(v) = \begin{cases} -D_{\mathrm{Eu}}(v, \mathrm{CSF\,\&\,GM, CSF, \&\,BG}, 1) & , \mathrm{if} \;\; GM(v) > 0 \;\&\; CSF(v) > 0 \\ D_{\mathrm{Eu}}(v, \mathrm{GM} > 0, \mathrm{CSF\&BG}, F_{\mathrm{CSF}}) & , \mathrm{if\,GM}(v) > 0 \\ 0 & , \mathrm{otherwise} \end{cases}, \tag{6}$$

where BG (background) describes all voxels that contain no tissue. The cortical thickness map GMT$_{\mathrm{I}}$ is initialized as a modified version of the WMD, because the WMD describes the distance only to the center of a GM voxel. GM voxels with more than 50% CSF need additional correction by the CSFD, in which the minimum correction is half of the voxel resolution *res*:

$$GMT_I(v) = WMD(v) + \min(CSFD(v), res/2). \tag{7}$$

Let N_{26} be the 26-neighborhood of a voxel v, and D_{26} the associated distance of v to its neighbors. A voxel $n \in N_{26}(v)$ is a successor of the voxel v if the WM distance of s meets the following conditional:

$$\%succ(v,n) = \begin{cases} 1 & , if (WMD(v) + a_1 * D_{26}(n)) < WMD(n) < (WMD(v) + a_2 * D_{26}(n)) \\ 0 & , otherwise \end{cases} \tag{8}$$

where $0 < a_1 \leq 1 \leq a_2 < 2$ are weights depending on the used distance metric; these weights allow the inclusion of more thickness information from neighboring voxels to achieve a smoother thickness map. If there are no successors, then v is a border voxel and the WM distance sets its thickness. The lower threshold a_1 defines the boundary between siblings and successors, whereas the higher threshold a_2 is a limit for direct successors. An a_1 threshold that is too low will create too many siblings and lead to smoother results, while an a_1 threshold that is too high will lead to coarser results. Likewise, an a_2 threshold that is too low will exclude more neighbors of v from the successor relationship and lead to less smooth images and in the worst-case to a breaking of the projection because all possible successors are excluded, whereas an a_2 threshold that is too high will lead to oversmoothed results with overestimation in gyral regions. For a quasi-Euclidean metric, which is not useful for cortical thickness but acceptable for the PP map, a_1 and a_2 are equal and can be set by the distance of v to its neighbors. Good results with minimal smoothing were achieved using $a_1 = 0.5$ and $a_2 = 1.25$. If there are no successors, then v is a border point and the WM distance sets its thickness, else it uses the mean of all successors:

$$pt(v) = \frac{\sum_{n \in N_{26}(v)} succ(v,n) * GMT_I(n)}{\sum_{n \in N_{26}(v)} succ(v,n)}. \tag{9}$$

The initial thickness GMT_I can now be used to estimate the final projection-based thickness map GMT_P, by projecting the values over the GM region:

$$GMT_P(v) = \max(GMT_I(v), pt(v)), \tag{10}$$

This mapping can be done in $O(n)$ time using the same principle Q5 described for voxel-based distance calculation (Rosenfeld and John, 1966). To reduce overestimations in the GMT_P map due to GM fragments such as blood vessels or dura mater, the direct thickness map:

$$GMT_D(v) = CSFD(v) + WMD(v), \tag{11}$$

is used to create the final thickness map:

$$GMT_F(v) = \min(GMT_P(v), GMT_D(v))/res, \tag{12}$$

that is corrected for the voxel resolution *res*. The percentage position map PP can now be described as:

$$PP(v) = (GMT_F(v) - WMD(v)/res))/GMT_F(v) + (SEG_{PF}(v) \geq 2.5). \tag{13}$$

Finally, the CS is generated from the PP map and reduced to around 300,000 nodes using standard Matlab functions. Each vertex of the mesh is assigned a thickness value via linear interpolation of the closest GM thickness map values. Fig. 3 shows the flow diagram of our method and illustrates the idea for most relevant examples in 2D.

PBT was used to reconstruct problematic regions in an additional preprocessing step that estimates the cortical thickness in the GM with flipped boundaries. These problematic regions are those that are highly susceptible to errors due to the PVE, which creates problems in both gyral and sulcal regions. In the gyral case, thin WM structures are blurred rather than the CSF blurring that occurs in narrow sulcal regions. This occurs most frequently in the superior temporal gyrus, the cingulate gyrus, and the insula, and may be addressed similarly to the idea proposed in (Cardoso et al.) for segmentation refinement. If a voxel of the inverse thickness map has lower thickness than the original thickness map and if the thickness of both is larger than 2 mm while SSEG > 2.0, we expect that the inverse thickness map has identified a gyrus that is blurred by the PVE. For these blurred regions, the thickness and percentage position of the inverse maps are used.

Laplacian-based thickness

The Laplacian approach requires an explicit sulcal reconstruction step (Jones et al., 2000; Tosun et al., 2004) that uses a skeleton map to reconstruct the outer boundary in blurred regions of the segment image SEG_{PF} (Fig. 4b2) by changing the tissue class of the reconstructed boundary voxels from GM to CSF resulting in a map SEG_{PFS} (Figs. 4b3, 4a). To create the skeleton map S, we first generate WM and CSF distance maps with the same distance measure used for PBT to allow asymmetrical structures. We then find areas with high divergence of the gradient field, resulting in a map SR. This map is normalized within a low and a high boundary $s_{low} = 0.5$ and $s_{high} = 1.0$ resulting in the skeleton map S (Bouix and Kaleem, 2000), with & as a logical AND operator: Q6

$$SR = \nabla\Delta(WMD)$$
$$S = \left(SR * \left((SR > s_{low}) \& \left(SR < s_{high}\right)\right) - s_{low}\right) * \left(s_{high} - s_{low}\right) + \left(SR \geq s_{high}\right). \tag{14}$$

The skeleton map accurately represents the sulci that have been blurred in the tissue segmentation process. We correct all voxels of $SEG \geq 1$ by:

$$SEG_{PFS} = SEG_{PF} - \max(1, 2 - S) * (SEG_{PF} \geq 1)) \tag{15}$$

(Fig. 4b3). The changing of GM voxels to CSF voxels leads to an underestimation of the GM volume and local thickness, which will be considered later. The corrected segment map SEG_{PFS} can now be used to solve the Laplace equation between the GM/WM and GM/CSF boundary:

$$\nabla^2\psi = \frac{\partial\psi}{\partial x^2} + \frac{\partial\psi}{\partial y^2} + \frac{\partial\psi}{\partial z^2} = 0. \tag{16}$$

The above equation is solved iteratively using an initial potential image with Dirichlet boundary conditions. The WM ($SEG_{PFS} \geq 2.5$) forms the higher potential boundary with values of 1, whereas the CSF ($SEG_{PFS} \leq 1.5$) represents the lower potential boundary with values of 0. To accelerate convergence, all GM voxels are initialized with a potential of 0.5. Eq. (17) is applied only to GM voxels ($SEG_{PFS} > 1.5$ and $SEG_{PFS} < 2.5$) and simply describes the mean of the six direct neighbors of a voxel:

$$\psi_i + 1(x,y,z) = \frac{1}{6} * \begin{bmatrix} \psi_i(x + \Delta x, y, z) + \psi_i(x - \Delta x, y, z) + \\ \psi_i(x, y + \Delta y, z) + \psi_i(x, y - \Delta y, z) + \\ \psi_i(x, y, z + \Delta z) + \psi_i(x, y, z - \Delta z) \end{bmatrix}. \tag{17}$$

The solution has converged when the error $\varepsilon = (\psi_{i-1} - \psi_i)/\psi_{i-1}$ is below a threshold value of 10^{-3}. After generating the potential

Please cite this article as: Dahnke, R., et al., Cortical thickness and central surface estimation, NeuroImage (2012), http://dx.doi.org/10.1016/j.neuroimage.2012.09.050

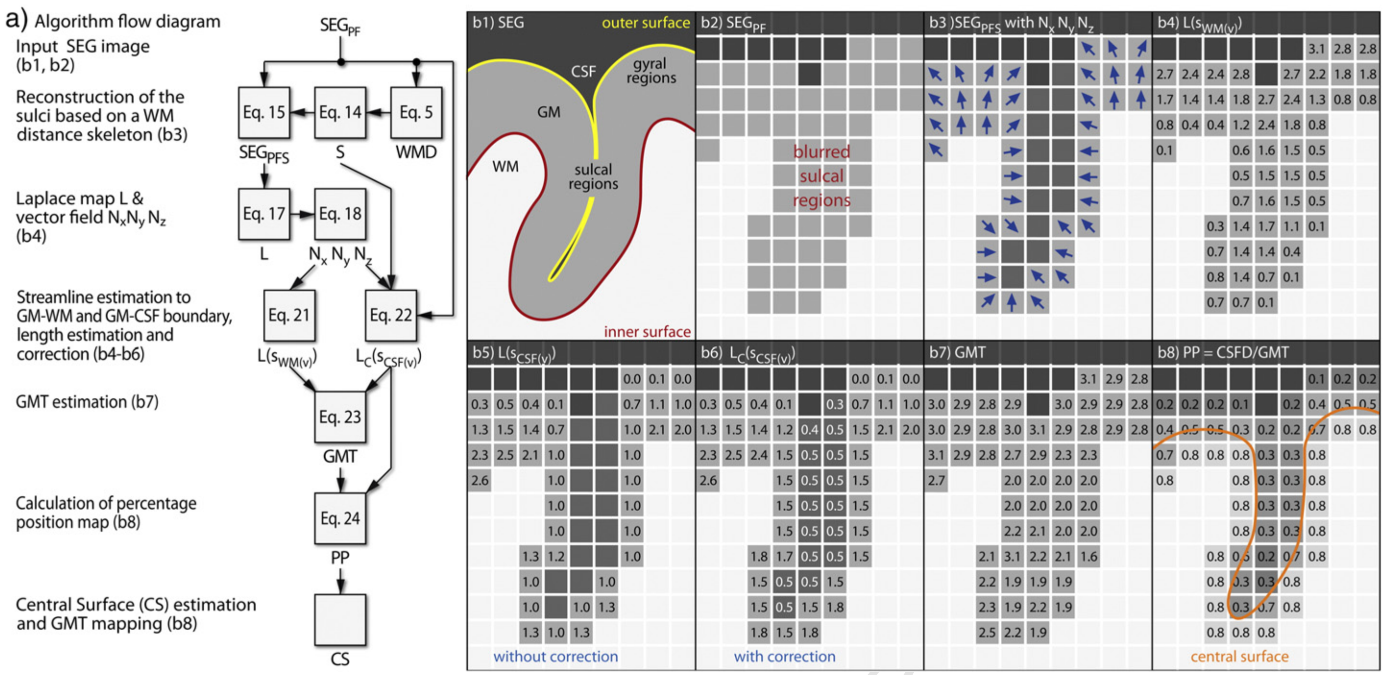

Fig. 4. Subfigure (a) shows a flow diagram of the Laplacian approach, where subfigure (b1–b8 with simplified titles) shows 2D illustrations of the volume maps of subfigure (a). First, a skeleton based on the WM distance map (see Fig. 3b2) is used to reconstruct blurred sulcal regions (b1–b3). Next, the Laplace equation is solved in the GM area and a vector field N is generated (b3). This vector field allows the creation of streamlines that follow the vectors to each boundary to measure the distance (b4–b6). To avoid an underestimation due to sulcus reconstruction (b5), the CSF distance $L(s_{CSF}(v))$ was corrected for changes from the sulcus reconstruction (Eq. (22)). The addition of both distance maps gives the cortical thickness map GMT that allows the creation of the percentage position map PP, which in turn is used to create the CS and map cortical thickness onto the surface.

image, we calculate the gradient field N of the Laplace map as the simple normalized two-point difference for each dimension. For example, along the x-direction the normalized potential difference N_x is calculated as follows:

$$N_x = (\Delta\psi/\Delta x)/\sqrt{(\Delta\psi/\Delta x)^2 + (\Delta\psi/\Delta y)^2 + (\Delta\psi/\Delta z)^2}, \tag{18}$$

$$\Delta\psi(x,y,z)/\Delta x = [\psi(x+\Delta x,y,z) - \psi(x-\Delta x,y,z)]/2. \tag{19}$$

Three normalized potential difference maps are then created: N_x, N_y, and N_z (Fig. 4b3 — blue vectors). From these maps, we calculate gradient streamlines for every GM voxel. A streamline s is a vector of points $s_1,\ldots,s_n$ that describes the path from the starting point s_1 to a border. The following point, s_{i+1}, of s_i is estimated by using the Euler's method, or by adding the weighted normalized gradient $N(s_i)$ to s_i:

$$s_{i+1} = s_i + hN_x(s_i) + hN_y(s_i) + hN_z(s_i). \tag{20}$$

The weight h describes the step size of the streamline calculation and was set to 0.1 mm as a compromise between speed and quality. For every GM voxel v, we calculate the streamline $s_{WM}(v)$ starting at the position of v to the WM boundary and other streamline $s_{CSF}(v)$ from v to the CSF boundary. To calculate $s_{CSF}(v)$, it is necessary to use the inverse gradient field. The length of a streamline $L(s)$ can be found by summing the Euclidean distance of all points s_i to their successor s_{i+1}:

$$L(s) = \sum_{i=1}^{n-1}\sqrt{\left(s_{i+1,x}-s_{i,x}\right)^2 + \left(s_{i+1,y}-s_{i,y}\right)^2 + \left(s_{i+1,z}-s_{i,z}\right)^2}. \tag{21}$$

We correct for errors introduced by the skeleton S using the volume difference between the uncorrected tissue segment SEG_{PF} and the corrected tissue segment SEG_{PFC}.

$$L_C(s) = L(s) + SEG_{PF}\left(s_{n,x},s_{n,y},s_{n,z}\right) - SEG_{PFC}\left(s_{n,x},s_{n,y},s_{n,z}\right). \tag{22}$$

The summation of the length of both streamlines $s_{WM}(v)$ and $s_{CSF}(v)$ gives the GM thickness at voxel v (Figs. 4b5 and b6). The RPM can also be calculated using the values for the lengths of $s_{WM}(v)$ and $s_{CSF}(v)$, with all WM voxels set to one:

$$GMT(v) = L\left(s_{WM(v)}\right) + L_C\left(s_{CSF(v)}\right), \tag{23}$$

$$PP(v) = L_C\left(s_{CSF(v)}\right)/GMT(v) + (SEG_{PFC}(v) > 2.5). \tag{24}$$

(Figs. 4b7 and b8). Finally, the CS surface is generated at a resolution of 0.5 mm from the PP map and reduced to around 300,000 nodes using standard Matlab functions. Each vertex of the mesh is assigned a thickness value via a linear interpolation of the closest GMT map values.

Spherical phantoms

A variety of spherical phantoms were used for validation. For the standard gyral case, the spherical phantom consisted of a cortical GM ribbon around a WM sphere in the center of the tissue map (Fig. 5). To explore the ability to reconstruct blurred sulcal regions, a second spherical phantom was constructed such that it contained a cortical GM ribbon sandwiched in between two WM regions: the center sphere and an outer shell. Between the ribbon boundaries, a small gap allows testing of the influence of the presence of CSF. To simulate asymmetrical structures, the size of the second ribbon was defined as a ratio of the size of the first GM ribbon. To realize this phantom with PVE, a distance map SPD that measures the distance

Please cite this article as: Dahnke, R., et al., Cortical thickness and central surface estimation, NeuroImage (2012), http://dx.doi.org/10.1016/j.neuroimage.2012.09.050

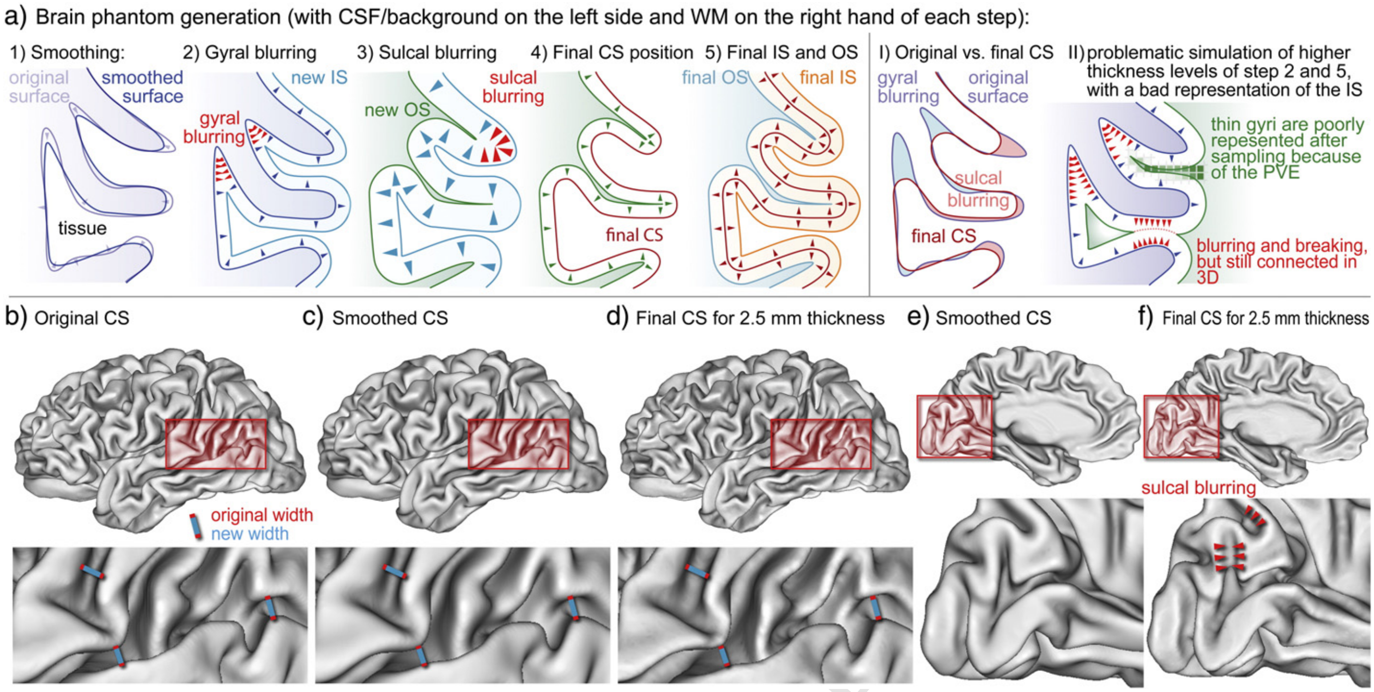

Fig. 5. Spherical phantom validation matrix: Two spherical phantom types – one for the gyral case (CGW) and one for the blurred sulcal case (WGW) – were used with different parameters for each method. The rows and columns are used to describe curvature (given by inner radius) and thickness values under varying conditions (see Table 1 and Fig. 7).

from the center of the volume at a resolution of $1\times1\times1\ \mathrm{mm}^3$ is used to create the tissue map TS:

$$T_{PVE}(v,r)=\begin{cases}1 & ,\ if\ \ SPD(v)\le(r-0.5)\\ r+0.5-SPD(v) & ,\ if\ \ SPD(v)>(r-0.5)\ \&\ SPD(v)<(r+0.5),\\ 0 & ,\ if\ \ SPD(v)\ge(r+0.5)\end{cases}\tag{25}$$

$$\begin{aligned}TS_{PVE}(v,r,t,sw,rsp) &= \mathrm{inner}-\mathrm{WM}-\mathrm{sphere}+\mathrm{inner}-\mathrm{GM}-\mathrm{sphere}+\mathrm{CSF}-\mathrm{sphere}+\\ &\mathrm{outer}-\mathrm{GM}-\mathrm{sphere}+\mathrm{outer}-\mathrm{WM}-\mathrm{sphere}\\ &=T_{PVE}(v,r)+T_{PVE}(v,r+t)+1\\ &+(1-T_{PVE}(v,r+t+sw))+\\ &(1-T_{PVE}(v,r+t+sw+((t/rsp)*(1-rsp))))\end{aligned}\tag{26}$$

where v is voxel of TS, r gives the inner boundary radius, t describes the thickness, sw is the sulcus width, and rsp is the relative sulcus position. Thickness is only evaluated for the inner ribbon because for asymmetrical structure the outer ribbon has a different thickness and curvature.

Table 1 shows the values of each parameter to be tested. To test one parameter, all other parameters were fixed to standard values. The range of values chosen for the parameters was based on anatomical and technical considerations.

Brain phantoms

To ensure an equal thickness for the brain phantom, it is necessary to expand sulcal regions such that they are able to achieve full thickness without intersections. To accomplish this, a CS of a healthy adult test subject was generated with Caret (Van Essen et al., 2001) and manually corrected for geometrical and topological errors (Fig. 6b). Twenty iterations of weighted nearest neighbor surface-based smoothing (included in the Caret package) were used to remove high frequency structures that can lead to problems in later manipulation steps (Figs. 6c, a1). A graph-based distance measure D_{gb} is used to create a distance map that describes the distance with sub-voxel accuracy to a given iso-surface that was generated via Matlab iso-surface functions. The initial surface was linearly interpolated once to reduce missed measurements. This distance map allows finding the new inner boundary at half distance (Fig. 6a2). From this new inner boundary, we estimated the new outer boundary based on the distance map generated from the inner boundary. If a sulcus is too small to allow increased thickness without intersections, then it is blurred (Fig. 6a3). From this new outer boundary, a new distance map allows the creation of the final central boundary (Fig. 6a4). The distance map BPD from the central boundary now allows the creation of a segment image

Table 1
Overview of parameters for the brain phantom test cases. For each test case, the anatomically expected range of each parameter was tested while all other parameters remained constant. The bracketed values give the number of test cases for each parameter. In most cases, only one default value was used. Because the cortex contains both blurred (CGW) and non-blurred (WGW) regions, both cases were tested. When testing sulcal width and position, more than one default value was necessary due to high variance in the results. For example, a symmetrical sulcus will produce better results than an asymmetric sulcus.

Parameter	Curvature	Thickness	PVE vs no PVE	V vs. S	Type	Sulcus width	rel. sulcus pos
Ranges	1.0:0.01:5.0 (401)	0.0:0.01:5.0 (501)	0 1 (2)	V S (2)	CGW WGW (2)	0.0:0.01:2.0 (200)	0.2:0.001:0.8 (601)
Defaults	2.5 (1)	2.5 (1)	1 (1)	S (1)	CGW WGW (2)	0.0:0.50:1.0 (3)	0.3:0.2:0.7 (3)

Please cite this article as: Dahnke, R., et al., Cortical thickness and central surface estimation, NeuroImage (2012), http://dx.doi.org/10.1016/j.neuroimage.2012.09.050

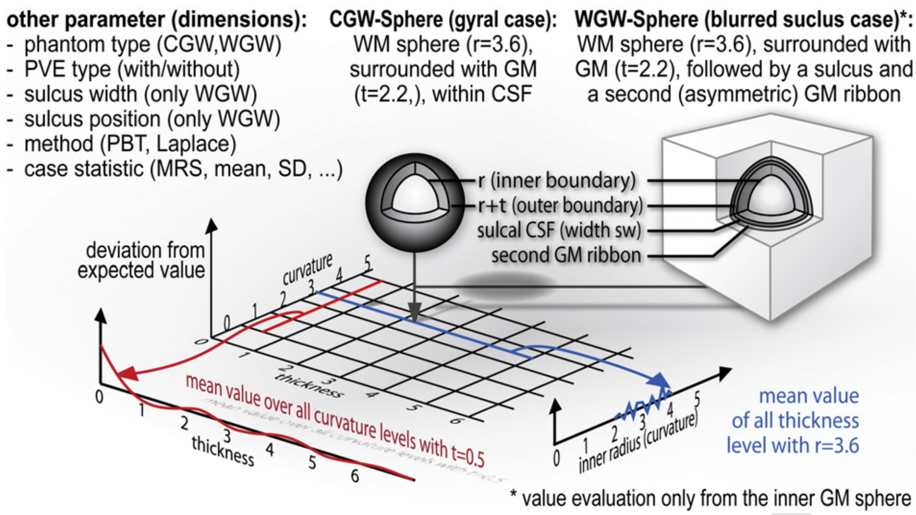

Fig. 6. Brain phantom generation: Subfigure (a) illustrates the generation process for the brain phantom, the difference between the original and final surface (a.I), and problems for higher thickness levels (a.II), whereas (b) to (f) show the changes from the individual surface to the brain phantom. A smoothed individual surface of a healthy adult (a.1) is transformed by distance operations to a surface that allows the creation of a *t*-mm thick cortical ribbon (a.5). This process removes high-frequency WM structures (a.2) and enlarges sulcal regions (a.3) to ensure an actual thickness level between 0.5 and 4.0 mm. Larger thicknesses destroy most of sulcal structures of a normally folded brain (a.II).

with WM, GM, and CSF (Fig. 5a5) (for a resolution of $0.5\times0.5\times0.5\ \text{mm}^3$):

$$TB_{PVE}(v,r)=\begin{cases}3 & ,\ if\ BPD(v)\geq(-t/2-0.25)\\ -t/2-0.25+BPD(v) & ,\ if\ BPD(v)<(-t/2-0.25)\ \&\ BPD(v)>(-t/2+0.25)\\ 2 & ,\ if\ BPD(v)\leq(-t/2+0.25)\ \&\ BPD(v)\geq(t/2-0.25)\\ t/2+0.25-BPD(v) & ,\ if\ BPD(v)<(t/2-0.25)\ \&\ BPD(v)>(t/2+0.25)\\ 1 & ,\ if\ BPD(v)\leq(t/2+0.25)\end{cases}. \tag{27}$$

The default parameters (2.5 mm thickness, $1\times1\times1\ \text{mm}^3$ resolution, 0% noise) were modified individually, resulting in 14 thickness levels, 9 noise degrees, and 7 isotropic and 7 anisotropic grid resolutions. The dataset is available under http://dbm.neuro.uni-jena.de/phantom/.

Collins phantoms

To test different thickness levels on one surface and stability for images interferences, 6 BrainWeb T1-weighted phantom datasets (1-mm resolution) with 1%, 3%, 5%, 7%, 9% noise and 20% inhomogeneity were compared to a dataset without noise and inhomogeneity (Collins et al., 1998).

Real data

The sample data set included 12 brain scans of the same healthy adult subject performed on two different 1.5 T Siemens Vision scanners within one year. Both scanners used 3D magnetization prepared gradient echo (MP-RAGE) T1-weighted sequences of 160 sagittal slices with voxel dimensions $1\times1\times1$ mm and FOV = 256 mm. Scanner 1 parameters were TR/TE/FA = 11.4 ms/4.4 ms/15°, and Scanner 2 parameters were TR/TE/FA = 15 ms/5 ms/30°.

Each reconstructed surface of the 12 scans was compared to an average scan to estimate the surface reconstruction and thickness errors, similar to the analysis used for the Collins phantom. Ideally, all reconstructions should be identical, and they should produce identical thickness measurements.

Results

Four different test matrices were used to validate PBT; these results were then compared to the Laplacian approach and, wherever applicable, to FreeSurfer. The first test consisted of the set of spherical phantoms, which were used to test the approaches over a wide set of parameters under simple but precise conditions. The second test, consisting of the brain phantoms, was used to explore the performance of the approaches under the more realistic condition of a highly convoluted surface with equal thickness. For the third test, we used the Collins phantom with different noise levels, both to add more realism and to directly compare the results to the FreeSurfer software package. Finally, we used real MR data of one subject for a test–retest of all three methods.

Spherical phantoms

Over all test parameters, PBT shows better results than the Laplacian approach for both thickness estimation and surface generation (Fig. 7a). As expected, both methods have higher RMS error for thickness estimation than for surface generation, both produce better results with PVE, and both perform better for the simpler gyral case compared to the sulcal case. The voxel-based results of the Laplacian approach are much worse than after projection to the surface, whereas PBT produced equally accurate results due to the smoothness parameter of the projection. Compared to gyral regions, sulcal regions show higher RMS error, which is strongly related to the width of the sulcal gap and its relative position.

Predicted by the sampling theorem, both show a strong increase of RMS error below sampling resolution for thickness measurements, but not for surface generation (Figs. 7b and c).

Furthermore, the Laplacian approach had larger fluctuations of error across the test cases. Relatively small variations of the test parameters led to vastly different error values (Fig. 7c above 2.5 mm). This strong variation can only be found if the step size of the parameter is very small — around 0.01 mm. Especially, asymmetrical structures (Fig. 7d) and small sulcal gaps (Fig. 7e) vastly increase the RMS error of the Laplacian approach.

For the Laplacian approach, we were able to produce good results such as those published in the literature only for cases with relatively large CSF regions and low asymmetry, whereas PBT produced more exact and stable results over the full range of test parameters.

Brain phantoms

For the brain phantoms, if the two approaches are compared, the PBT method has much lower RMS error for the thickness measurements and

Please cite this article as: Dahnke, R., et al., Cortical thickness and central surface estimation, NeuroImage (2012), http://dx.doi.org/10.1016/j.neuroimage.2012.09.050

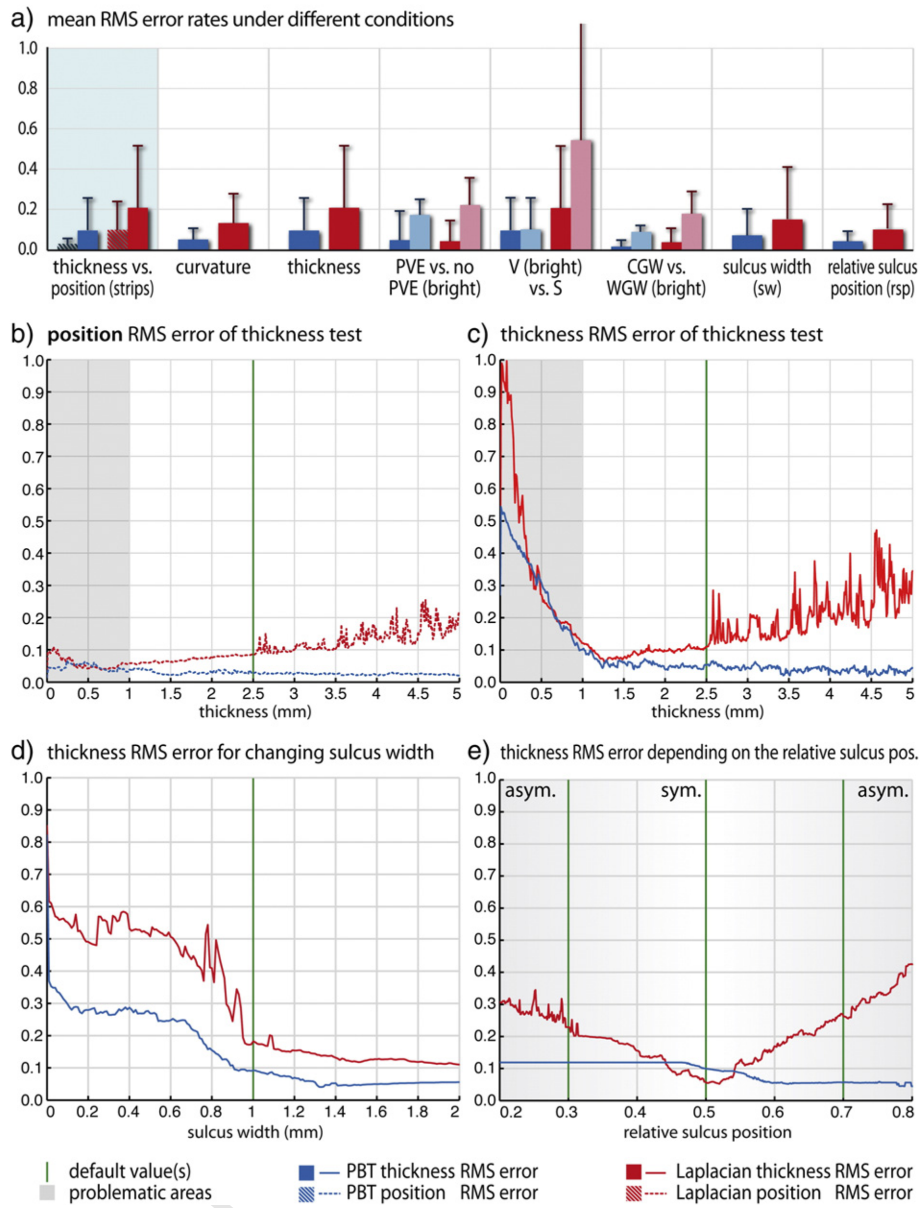

Fig. 7. Spherical phantom: PBT results in lower RMS error for all test categories, compared to the Laplacian approach (a). Below sampling resolution, both methods show a predictable increase of thickness measurement error due to the sampling theorem (c), whereas the position error stays stable (b). Most errors happen for sulcal cases with low sulcus width (d) and higher asymmetries (e).

similar RMS error for the surface position compared to the Laplacian method (Fig. 8). The errors occur mostly in sulcal regions where the sulcus reconstruction step cut strongly into the fundi of the sulci such that that a complete correction was not possible (Fig. 8a). However, using a weaker sulcus reconstruction step or stronger corrections led to thickness overestimation, more defects, and greater RMS errors, thus it was impossible to circumvent this problem. Generally, the largest errors occurred for anisotropic resolutions, thickness levels below the sampling resolution, and higher noise levels. It can be assumed that these factors would apply to any cortical data set, and thus should be considered before applying any cortical reconstruction method.

Collins phantom

The advantage of using an additional Collins phantom is that the two approaches described here (PBT and Laplacian) can be compared to a commonly used approach for both reconstructing cortical surfaces and measuring thickness, e.g., FreeSurfer. To summarize the findings, the PBT approach had comparable or lower RMS error compared to both the Laplacian and FreeSurfer approaches (Fig. 7, Supplementary Fig. A1). If the noise level is increased, all thickness measures also had increasing error. A two-sample unpaired *t*-test showed no significant differences of the RMS position error between PBT and Laplacian ($t=-0.048$, $df=8$, $p=0.963$) and PBT and FreeSurfer ($t=1.348$, $df=8$, $p=0.215$). A significant difference in thickness between PBT and Laplacian was found ($t=-2.95$, $df=8$, $p=0.019$), but not for PBT vs. FreeSurfer ($t=-0.944$, $df=8$, $p=0.374$). Furthermore, the PBT method provides an advantage in terms of reduced numbers of topological defects (an average of 15.1 for PBT, compared to 28.2 for Laplacian and 18.5 for FreeSurfer). PBT had significantly fewer defects compared to the Laplacian approach ($t=-8.656$, $df=10$, $p<0.001$), but not compared to FreeSurfer ($t=-1.481$, $df=10$, $p=0.182$). The defects associated with the Laplacian and PBT approaches were mostly bridges between two gyri and were removed by the topology

Please cite this article as: Dahnke, R., et al., Cortical thickness and central surface estimation, NeuroImage (2012), http://dx.doi.org/10.1016/j.neuroimage.2012.09.050

ARTICLE IN PRESS

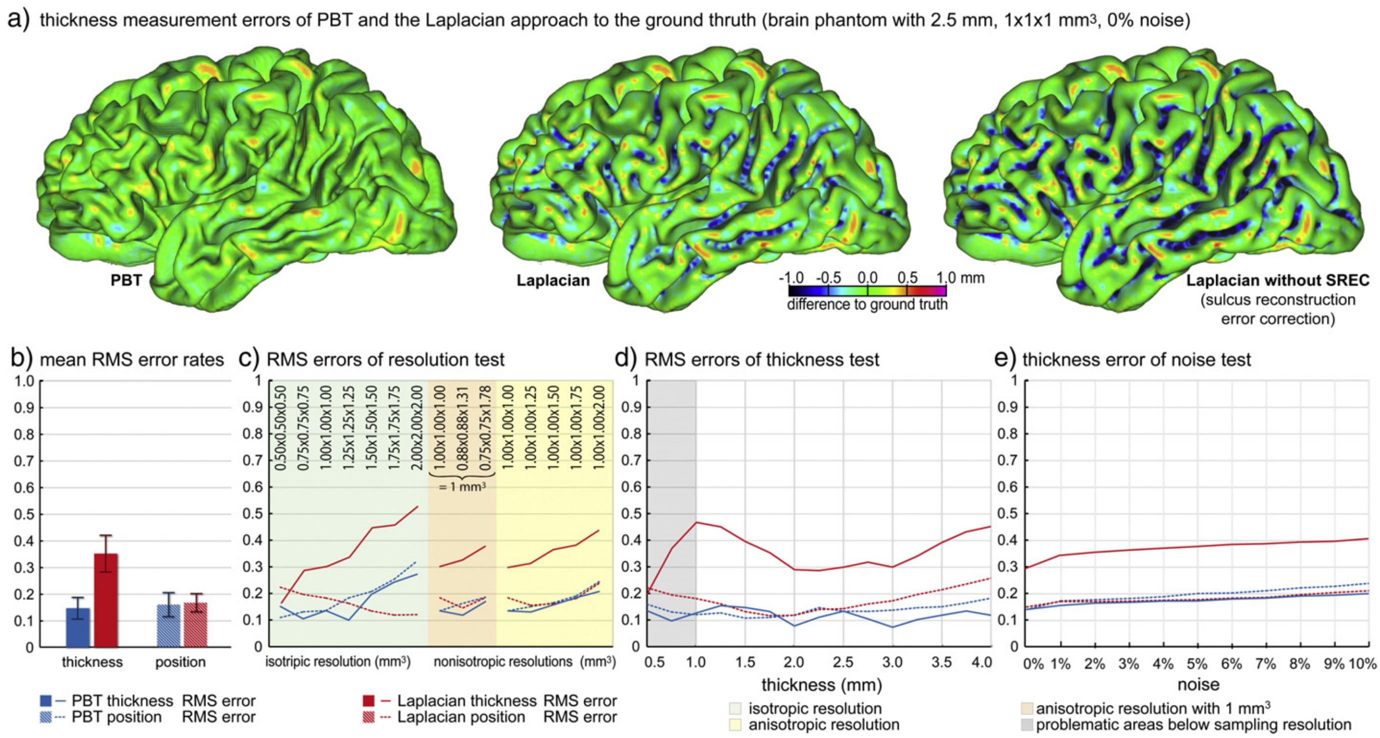

Fig. 8. Brain phantom: Subfigure (a) shows the resulting surfaces for a simulated thickness of 2.5 mm, with an isotropic resolution of $1 \times 1 \times 1$ mm^3 and no noise. PBT produced overall good results (left), whereas the Laplacian approach showed strong underestimation in sulcal regions due to the sulcus reconstruction step (right), even if sulcus error correction was used (middle). The Laplacian approach (b — red) produced much higher thickness RMS errors than PBT (b — blue). Low sample resolution, anisotropic resolutions, and noise may increase the RMS error for both thickness measurements as well as CS position (c–e). (For interpretation of the references to color in this figure legend, the reader is referred to the web version of this article.)

correction. These results were highly dependent upon the quality of the initial tissue segmentation, the implications of which are discussed more fully in the Discussion section (Fig. 9).

Inline supplementary Fig. A1 can be found online at http://dx.doi.org/10.1016/j.neuroimage.2012.09.050.

Twelve scans of one subject

As a final approach for quantifying the performance of three approaches (PBT, Laplacian, FreeSurfer), we analyzed twelve separate scans of a single brain, then compared the results to an averaged scan of the same brain. Since the elapsed time between scans was less than one year, cortical thickness should be unchanged. Again, the PBT approach provided some advantages over the other methods (Fig. 10, Supplementary Fig. A2). First, the PBT approach is comparable to or better than other approaches in terms of the RMS thickness measurement errors (Fig. 10c; PBT: 0.39 ± 0.02 mm; Laplacian: 0.64 ± 0.02 mm; FreeSurfer: 0.53 ± 0.05 mm), and the RMS position error of the CS reconstructions was similar to the other two approaches (Fig. 10d; PBT: 0.50 ± 0.05 mm; Laplacian: 0.54 ± 0.05 mm; FreeSurfer: 0.60 ± 0.23 mm). There was no significant difference in the RMS position error between PBT and the Laplacian approach ($t = -1.922$, $df = 22$, $p = 0.067$) and PBT and FreeSurfer ($t = -1.409$, $df = 22$, $p = 0.172$), whereas the difference of the RMS thickness error was significant ($t = -8.177$, $df = 22$, $p < 0.001$). A major difference between the PBT and Laplacian approaches compared to FreeSurfer is a general underestimation of thickness in the motor cortex (Fig. 10b). Finally, the PBT approach produced far fewer topological defects per hemisphere compared to Laplacian ($t = -6.036$, $df = 24$, $p < 0.001$) and FreeSurfer ($t = -4.030$, $df = 24$, $p < 0.001$) (Fig. 10a; PBT: 21.5; Laplacian: 34.6; FreeSurfer: 54.6).

Inline supplementary Fig. A2 can be found online at http://dx.doi.org/10.1016/j.neuroimage.2012.09.050.

All calculations were done on an iMac 3.4 GHz Intel Core i7 with 8 GB RAM and Matlab 7.12. For both hemispheres with a resolution of 0.5 mm and with topology error correction, PBT needed around 20 min, whereas the Laplacian approach takes around 2 h. Although the FreeSurfer processing pipeline is structured differently than the PBT and Laplacian approaches, rendering comparison difficult, an estimate of the time to perform cortical reconstruction and thickness measurement is several hours.[6]

Discussion

For nearly all test cases, PBT had much lower thickness and position errors than the Laplacian approach, because PBT uses an inherent model that detects sulci, whereas the Laplacian method requires an explicit sulcus reconstruction step that changes the tissue class of sulcal voxels and may lead to the introduction of additional errors, even if these tissue class changes are compensated for within the algorithm. The different tests of the spherical phantom clearly show that the strong errors of the Laplacian approach only happen in asymmetric sulcal regions, although both methods are based on the same Eikonal distance measure that accounts for the sulcal gap. Because the real cortex also contains asymmetrical structures, it is important that the thickness measure is able to accurately evaluate these asymmetries (Das et al., 2009; Fischl and Dale, 2000; Kim et al., 2005). In addition, the brain phantoms indicate errors on the fundi of the sulci for the Laplacian method, whereas the continuous model of PBT allows a stable estimation over the whole cortex.

The correct reconstruction of blurred sulci is still a challenging process, since the result depends strongly on the used method and its parameters (Acosta et al., 2008, 2009; Cardoso et al.; Dale et al., 1999; Das et al., 2009; Han et al., 2004; Hutton et al., 2008; Kim et

[6] https://surfer.nmr.mgh.harvard.edu/fswiki/ReconAllRunTimes

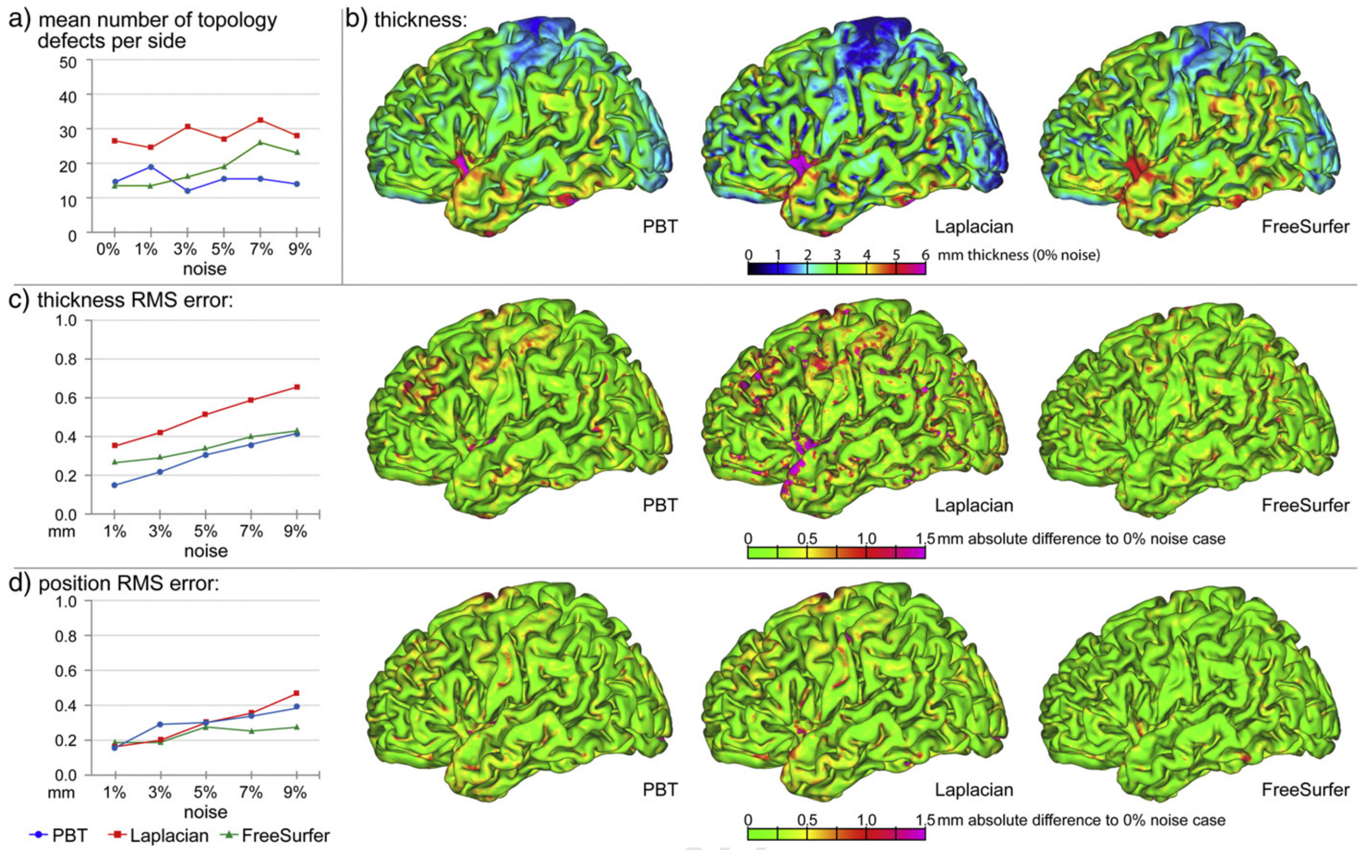

Fig. 9. Collins phantom: Diagram (a) shows the mean number of defects per hemisphere for PBT (blue), Laplacian (red), and FreeSurfer (green). Subfigures (b–d) show the ground truth surface of the Collins phantom noise test for PBT (left surface), Laplacian (middle surface), and FreeSurfer (right surface), in which the color map codes the cortical thickness of the ground truth surface (b), the mean thickness RMS error of all noise levels compared to the ground truth surface (c), and the mean distance RMS error of all noise levels to the ground truth surface (d). A supplementary figure, including medial and lateral views of both hemispheres, is available online. (For interpretation of the references to color in this figure legend, the reader is referred to the web version of this article.)

al., 2005; MacDonald et al., 2000; Scott and Thacker, 2005). The shown results of the different methods allow only a rough impression about the quality of the sulcus reconstruction step, by showing that the modeling of sulcal blurring leads to results that are closer to the simulated cortical thickness. Most differences in these methods are visible especially on the fundi of the sulci, which is where some approaches have thickness over- or underestimation. Although other authors, i.e. (Das et al., 2009; Hutton et al., 2008; Kim et al., 2005), illustrate the reconstruction of blurred regions for principle examples, this is the first paper that introduces a way to numerically validate an algorithm using not only simple cases with well-known parameters and without fundi, but also for highly convoluted surfaces with fundi.

Compared to surface-based approaches, PBT does not need extensive surface deformation or self-intersection tests, which are necessary for both Freesurfer (Dale et al., 1999) and CLASP (Kim et al., 2005). In contrast to FreeSurfer, PBT is able to use tissue segmentation images produced using any segmentation approach, allowing a separate development of the segmentation algorithms and thus making this process more transparent. Furthermore, this allows the use of segmentation images for other imaging modalities such as T2, PD (Ashburner and Friston, 2005; Zhang et al., 2001), DTI (Liu et al., 2007), and other methods that take account of special contrast properties in disease states such as multiple sclerosis (Khayati et al., 2008; Wu et al., 2006), white matter hyper-intensities (Admiraal-Behloul et al., 2005; Gibson et al.), or tumors (Kaus et al., 2001; Prastawa et al., 2004), or for other species (Andersen et al., 2002). As a result, the input of PBT and other segment-based methods depends strongly on the results of the segmentation. The tests with the spherical and brain phantoms were independent from the segmentation process, because the segmentation images were directly simulated, whereas the Collins phantom and the real dataset include a segmentation step. Evidence of the strong influence of the segmentation algorithm on results may be seen with the Collins phantom. Since the tissue boundaries are simulated, these phantoms included artificially precise tissue classification and resulted in much more similar thickness measurements for all methods than for the real data set (especially in the motor cortex).

Furthermore, PBT allows a direct voxel-based analysis, potentially in combination with other voxel-based data (Hutton et al., 2009), and it may also be used to measure the thickness of the WM and CSF [HBM2010]. The voxel-based thickness estimation of PBT and other methods allows the easy creation of the central surface, which has better properties than the WM or pial surface. Previous approaches generally reconstruct a surface at a tissue boundary, which is either the WM surface or the pial surface. In one sense, such a reconstruction makes sense, since the intensity gradient in these regions can be used to estimate the position of the surface. However, due to the PVE, the boundaries often contain voxels with more than one tissue class and thus render it impossible to determine the precise location of the surface within that voxel. In the approach suggested here, the effect of PVE is somewhat reduced, since the central surface is reconstructed simply at the 50% distance boundary between the GM/WM and GM/CSF boundaries. This effect is responsible for the constant RMS position error below the sampling resolution, whereas thickness errors grow much stronger, because the PVE and neighbor information can only code the exact position of one boundary. For instance, for the 1D case of a voxel v and its left and right neighbors v_l and v_r, where $v=2.25$, $v_l=2$, and $v_r=3$, the WM boundary is exactly described between v and v_r, but if $v_l=1$, then there are two

Please cite this article as: Dahnke, R., et al., Cortical thickness and central surface estimation, NeuroImage (2012), http://dx.doi.org/10.1016/j.neuroimage.2012.09.050

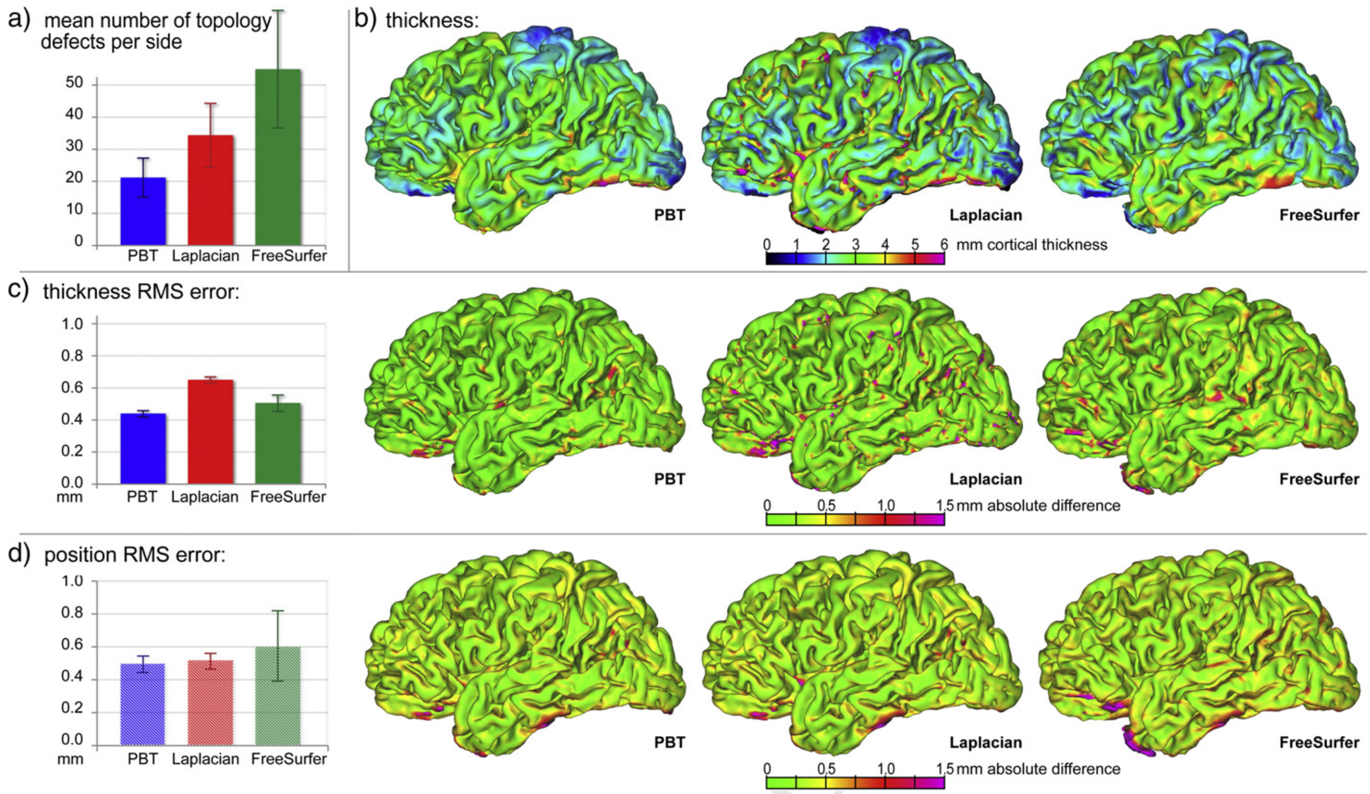

Fig. 10. Real data: Diagram (a) show the mean number of defects per hemisphere for PBT (blue), Laplacian (red), and FreeSurfer (green). Shown in (b–d) are PBT (left column), Laplacian (middle column), and FreeSurfer (right column) surfaces with (b) cortical thickness calculated for the average surface, (c) mean thickness RMS error of all scans compared to the thickness of the average surface, and (d) mean distance RMS error of all scans to the average surface. Strong differences are visible in the thickness measurements for the motor cortex, which depended mostly on the segmentation algorithm (VBM8) and thus was similar for PBT and Laplacian, whereas FreeSurfer used internal routines. A supplementary figure, including medial and lateral views of both hemispheres, is available online. (For interpretation of the references to color in this figure legend, the reader is referred to the web version of this article.)

boundaries within v and it is unclear how much GM is within v. It is possible that there is only GM and WM in v, the WM boundary is at the same position, and the CSF boundary is exactly between v and v_I. But it is also possible that there is some CSF in v, and v contains three tissue classes and both boundaries. As a result, thickness RMS errors grow strongly for thickness levels below the sampling resolution.

Independent of the chosen reconstruction method, the general structure of the CS lends advantages that do not exist in the other surface reconstructions. First, the CS has a lower “frequency” content, or fewer finely detailed regions, since it is the average of the WM structure with its strong gyri and the pial surface with its deep sulci. Due to this characteristic of the CS, it may have fewer topological defects and it tends to lose less anatomical detail when smoothed. Since brain surfaces usually must be smoothed to remove stair artifacts and noise, the CS provides a distinct advantage over the other reconstructions. Secondly, another advantage of the CS is that it may be directly reconstructed from the data and thus leads to a more uniform distribution of vertices across the surface, which may be perturbed in a method that uses a deformation process to reconstruct a surface at a tissue boundary.

Before performing intersubject comparisons, the brain surface meshes must usually be free of topological defects, and there are several approaches available to retrospectively correct topological errors either in volume space or directly on the surface (Kriegeskorte and Goebel, Q8 2001; Segonne et al., 2007; Shattuck and Leahy, 2001; Yotter et al., 2009, in press). Despite the availability of these correction methods, it is desirable to minimize both the size and number of topological defects, since non-idealities in the correction step can often introduce errors. In this respect, the PBT approach is the best choice, since it produced the lowest number of defects, and the defects were also relatively small. Despite using the same segmentation images, the Laplacian approach resulted in a large number of defects, mostly due to overestimation of thickness in sulcal regions and thus the formation of bridges. A detailed discussion of the corrections of topology defects via spherical harmonics can be found in (Yotter et al., in press). Q9

Necessity of a full phantom test suite

Comparing different software packages is never easy, because there will always remain some differences in processing the data, i.e. the restriction of FreeSurfer to 1.0 mm resolution for all volumes whereas PBT and the Laplacian approach can also use higher resolutions (here 0.5 mm). Especially, the different segmentation routines limited the comparison between FreeSurfer and both other approaches. Furthermore, all methods based on different thickness definitions can also lead to slightly different results (Lerch and Evans, 2005; MacDonald et al., 2000).

Because visual inspection of surfaces gives only subjective, badly reproducible, and often limited impressions of the reconstruction quality (Kabani et al., 2001; Xu et al., 1999), we developed a complete test suite containing several parameters that could be varied to fully characterize both surface reconstruction and thickness measurement approaches. Although previous approaches tested a small number of phantom objects (Acosta et al., 2009; Das et al., 2009; Miller et al., 2000), it is apparent from our results that it is necessary to test several parameters to gain information about an algorithm's performance, especially for special cases such as sulcal blurring. It could be further argued that simple geometrical objects provide only limited information about performance that cannot be extrapolated to cortical surfaces, thus it is appropriate to include pseudo-cortical surfaces with constant thickness over the whole cortex in the test suite. Unlike the previous methods (Liu et al., 2008), our cortical ribbon has an equal thickness and a more realistic structure. This constant thickness theoretically allows a direct comparison between different thickness measurement algorithms.

Using phantoms with equal thickness has the fundamental advantage that an equal ribbon allows theoretically similar thickness measurements, independent of the definition of the thickness measure. An illustration may clarify this point. Let t be the simulated thickness of a convoluted brain-like ribbon with equal thickness. First, for nearest-neighbor-based methods (i.e. T_{near} (MacDonald et al., 2000) for surface-based methods or nearest voxel for voxel-based methods), it is obvious that the nearest connection between both sides is given by the defined thickness t. Second, the T_{normal} (MacDonald et al., 2000) metric that measures the distance between both sides of the ribbon via the surface normal will measure the same thickness t, because of the well-defined structure of this ribbon, i.e., both boundaries have the same curvature by definition. Third, the streamline of the Laplacian approach will be equal to the surface normal, because they depend on the vector field given by the Laplace filter, which in turn depends on the curvature of both boundaries that are equal by definition. Fourth, the T_{link} (MacDonald et al., 2000) metric is defined for surfaces with equal numbers of vertices. Here, one surface is the result of a deformation of the other surface. The deformation is mostly based upon a field given by the intensity and/or by the surface normal or another Laplace vector field (Kim et al., 2005). Because the intensity is equal within the ribbon, only the surface normal or the vector field can be used for the deformation. As a result, the deformation is similar to the streamlines of the Laplacian approach that are similar to the surface normal.

The PVE approximation of the phantom generation based on distance maps leads to errors that depend on the resolution, the intensity (given by the distance), and the angles of the voxel to the coordinate system. The highest possible error for a resolution of $1\times1\times1$ mm^3 happens for a diagonal voxel within the middle slice, and is, with a volume error below 0.05 mm^3, comparable to other approximation methods (Acosta et al., 2009) in which the object is rendered first to $0.1\times0.1\times0.1$ mm^3 and then down-sampled back to $1\times1\times1$ mm^3. The advantage of using distance maps is the much lower memory demand and faster computation.

In the approach used here, segmentation images were directly simulated to avoid influences from the segmentation algorithm. However, it is possible to simulate a T1 image based on the tissue maps (Aubert-Broche et al., 2006), which would be useful for testing other methodological approaches using this test suite.

Conclusion

In this paper, we have presented a new method that allows for the simultaneous reconstruction of the CS and measurement of cortical thickness. Our PBT method is based on (probability) maps of a standard CSF–GM–WM tissue segmentation and has several advantages over the previous methods, such as direct estimation of the CS, comparable or lower errors, and fewer topological defects. We introduce a framework for thoroughly validating methods developed for surface reconstruction and thickness estimation, which quantifies the performance of the methods over a wide range of thickness levels and other parameters such as sampling resolution, noise, curvature, and PVE. The test framework explores performance both for the simple case of a sphere and also for nearly normal folded cortices with uniform thickness. Finally, we used real MR images from several scans of the same subject to compare both methods to FreeSurfer. The results indicate that the quality of our CS reconstructions and thickness estimations is comparable, and may be superior in certain respects, to other methods.

Acknowledgments

This work was supported by the following grants: BMBF 01EV0709 and BMBF 01GW0740.

References

Acosta, O., Bourgeat, P., Fripp, J., Bonner, E., Ourselin, S., Salvado, O., 2008. Automatic delineation of sulci and improved partial volume classification for accurate 3D voxel-based cortical thickness estimation from MR. Med. Image Comput. Comput. Assist. Interv. 11, 253–261.
Acosta, O., Bourgeat, P., Zuluaga, M.A., Fripp, J., Salvado, O., Ourselin, S., 2009. Automated voxel-based 3D cortical thickness measurement in a combined Lagrangian–Eulerian PDE approach using partial volume maps. Med. Image Anal. 13, 730–743.
Admiraal-Behloul, F., van den Heuvel, D.M., Olofsen, H., van Osch, M.J., van der Grond, J., van Buchem, M.A., Reiber, J.H., 2005. Fully automatic segmentation of white matter hyperintensities in MR images of the elderly. NeuroImage 28, 607–617.
Andersen, A.H., Zhang, Z., Avison, M.J., Gash, D.M., 2002. Automated segmentation of multispectral brain MR images. J. Neurosci. Methods 122, 13–23.
Ashburner, J., Friston, K.J., 2005. Unified segmentation. NeuroImage 26, 839–851.
Aubert-Broche, B., Evans, A.C., Collins, L., 2006. A new improved version of the realistic digital brain phantom. NeuroImage 32, 138–145.
Bouix, S.S., Kaleem, 2000. Divergence-based medial surfaces: ECCV, 1, pp. 603–618.
Cardoso, M.J., Clarkson, M.J., Ridgway, G.R., Modat, M., Fox, N.C., Ourselin, S., LoAd: A locally adaptive cortical segmentation algorithm. Neuroimage 56, 1386–1397.
Collins, D.L., Zijdenbos, A.P., Kollokian, V., Sled, J.G., Kabani, N.J., Holmes, C.J., Evans, A.C., 1998. Design and construction of a realistic digital brain phantom. IEEE Trans. Med. Imaging 17, 463–468.
Coupe, P., Yger, P., Prima, S., Hellier, P., Kervrann, C., Barillot, C., 2008. An optimized blockwise nonlocal means denoising filter for 3-D magnetic resonance images. IEEE Trans. Med. Imaging 27, 425–441.
Cuadra, M.B., Cammoun, L., Butz, T., Cuisenaire, O., Thiran, J.P., 2005. Comparison and validation of tissue modelization and statistical classification methods in T1-weighted MR brain images. IEEE Trans. Med. Imaging 24, 1548–1565.
Dale, A.M., Fischl, B., Sereno, M.I., 1999. Cortical surface-based analysis. I. Segmentation and surface reconstruction. NeuroImage 9, 179–194.
Das, S.R., Avants, B.B., Grossman, M., Gee, J.C., 2009. Registration based cortical thickness measurement. NeuroImage 45, 867–879.
Eskildsen, S.F., Ostergaard, L.R., 2006. Active surface approach for extraction of the human cerebral cortex from MRI. Med. Image Comput. Comput. Assist. Interv. 9, 823–830.
Eskildsen, S.F., Ostergaard, L.R., 2007. Quantitative comparison of two cortical surface extraction methods using MRI phantoms. Med. Image Comput. Comput. Assist. Interv. 10, 409–416.
Fischl, B., Dale, A.M., 2000. Measuring the thickness of the human cerebral cortex from magnetic resonance images. Proc. Natl. Acad. Sci. U. S. A. 97, 11050–11055.
Fischl, B., Sereno, M.I., Dale, A.M., 1999. Cortical surface-based analysis. II: inflation, flattening, and a surface-based coordinate system. NeuroImage 9, 195–207.
Fjell, A.M., Walhovd, K.B., Reinvang, I., Lundervold, A., Salat, D., Quinn, B.T., Fischl, B., Dale, A.M., 2006. Selective increase of cortical thickness in high-performing elderly–structural indices of optimal cognitive aging. NeuroImage 29, 984–994.
Gibson, E., Gao, F., Black, S.E., Lobaugh, N.J., Automatic segmentation of white matter hyperintensities in the elderly using FLAIR images at 3T. J. Magn. Reson. Imaging 31, 1311–1322.
Haidar, H., Soul, J.S., 2006. Measurement of cortical thickness in 3D brain MRI data: validation of the Laplacian method. J. Neuroimaging 16, 146–153.
Han, X., Pham, D.L., Tosun, D., Rettmann, M.E., Xu, C., Prince, J.L., 2004. CRUISE: cortical reconstruction using implicit surface evolution. NeuroImage 23, 997–1012.
Hofman, M.A., 1989. On the evolution and geometry of the brain in mammals. Prog. Neurobiol. 32, 137–158.
Hutton, C., De Vita, E., Ashburner, J., Deichmann, R., Turner, R., 2008. Voxel-based cortical thickness measurements in MRI. NeuroImage 40, 1701–1710.
Hutton, C., Draganski, B., Ashburner, J., Weiskopf, N., 2009. A comparison between voxel-based cortical thickness and voxel-based morphometry in normal aging. NeuroImage 48, 371–380.
Jones, S.E., Buchbinder, B.R., Aharon, I., 2000. Three-dimensional mapping of cortical thickness using Laplace's equation. Hum. Brain Mapp. 11, 12–32.
Kabani, N., Le Goualher, G., MacDonald, D., Evans, A.C., 2001. Measurement of cortical thickness using an automated 3-D algorithm: a validation study. NeuroImage 13, 375–380.
Kaus, M.R., Warfield, S.K., Nabavi, A., Black, P.M., Jolesz, F.A., Kikinis, R., 2001. Automated segmentation of MR images of brain tumors. Radiology 218, 586–591.
Khayati, R., Vafadust, M., Towhidkhah, F., Nabavi, M., 2008. Fully automatic segmentation of multiple sclerosis lesions in brain MR FLAIR images using adaptive mixtures method and Markov random field model. Comput. Biol. Med. 38, 379–390.
Kim, J.S., Singh, V., Lee, J.K., Lerch, J., Ad-Dab'bagh, Y., MacDonald, D., Lee, J.M., Kim, S.I., Evans, A.C., 2005. Automated 3-D extraction and evaluation of the inner and outer cortical surfaces using a Laplacian map and partial volume effect classification. NeuroImage 27, 210–221.
Kriegeskorte, N., Goebel, R., 2001. An efficient algorithm for topologically correct segmentation of the cortical sheet in anatomical mr volumes. NeuroImage 14, 329–346.
Kuperberg, G.R., Broome, M.R., McGuire, P.K., David, A.S., Eddy, M., Ozawa, F., Goff, D., West, W.C., Williams, S.C., van der Kouwe, A.J., Salat, D.H., Dale, A.M., Fischl, B., 2003. Regionally localized thinning of the cerebral cortex in schizophrenia. Arch. Gen. Psychiatry 60, 878–888.
Lee, J., Lee, J.M., Kim, J.H., Kim, I.Y., Evans, A.C., Kim, S.I., 2006a. A novel quantitative validation of the cortical surface reconstruction algorithm using MRI phantom: issues on local geometric accuracy and cortical thickness. Med. Image Comput. Comput. Assist. Interv. Int. Conf. Med. Image Comput. Comput. Assist. Interv. 9, 183–190.
Lee, J.K., Lee, J.M., Kim, J.S., Kim, I.Y., Evans, A.C., Kim, S.I., 2006b. A novel quantitative cross-validation of different cortical surface reconstruction algorithms using MRI phantom. NeuroImage 31, 572–584.

Please cite this article as: Dahnke, R., et al., Cortical thickness and central surface estimation, NeuroImage (2012), http://dx.doi.org/10.1016/j.neuroimage.2012.09.050

Lerch, J.P., Evans, A.C., 2005. Cortical thickness analysis examined through power analysis and a population simulation. NeuroImage 24, 163–173.

Liu, T., Li, H., Wong, K., Tarokh, A., Guo, L., Wong, S.T., 2007. Brain tissue segmentation based on DTI data. NeuroImage 38, 114–123.

Liu, T., Nie, J., Tarokh, A., Guo, L., Wong, S.T., 2008. Reconstruction of central cortical surface from brain MRI images: method and application. NeuroImage 40, 991–1002.

Lohmann, G., Preul, C., Hund-Georgiadis, M., 2003. Morphology-based cortical thickness estimation. Inf. Process. Med. Imaging 18, 89–100.

Luders, E., Thompson, P.M., Narr, K.L., Toga, A.W., Jancke, L., Gaser, C., 2006. A curvature-based approach to estimate local gyrification on the cortical surface. NeuroImage 29, 1224–1230.

MacDonald, D., Kabani, N., Avis, D., Evans, A.C., 2000. Automated 3-D extraction of inner and outer surfaces of cerebral cortex from MRI. NeuroImage 12, 340–356.

Mietchen, D., Gaser, C., 2009. Computational morphometry for detecting changes in brain structure due to development, aging, learning, disease and evolution. Front. Neuroinform. 3, 25.

Miller, M.I., Massie, A.B., Ratnanather, J.T., Botteron, K.N., Csernansky, J.G., 2000. Bayesian construction of geometrically based cortical thickness metrics. NeuroImage 12, 676–687.

Prastawa, M., Bullitt, E., Ho, S., Gerig, G., 2004. A brain tumor segmentation framework based on outlier detection. Med. Image Anal. 8, 275–283.

Rocha, K.R., Yezzi Jr., A.J., Prince, J.L., 2007. A hybrid Eulerian–Lagrangian approach for thickness, correspondence, and gridding of annular tissues. IEEE Trans. Image Process. 16, 636–648.

Rodriguez-Carranza, C.E., Mukherjee, P., Vigneron, D., Barkovich, J., Studholme, C., 2008. A framework for in vivo quantification of regional brain folding in premature neonates. NeuroImage 41, 462–478.

Rosas, H.D., Salat, D.H., Lee, S.Y., Zaleta, A.K., Pappu, V., Fischl, B., Greve, D., Hevelone, N., Hersch, S.M., 2008. Cerebral cortex and the clinical expression of Huntington's disease: complexity and heterogeneity. Brain 131, 1057–1068.

Rosenfeld, A.P., John, L., 1966. Sequential operations in digital picture processing. J. Assoc. Comput. Maschiery 13 (4), 471–494.

Sailer, M., Fischl, B., Salat, D., Tempelmann, C., Schonfeld, M.A., Busa, E., Bodammer, N., Heinze, H.J., Dale, A., 2003. Focal thinning of the cerebral cortex in multiple sclerosis. Brain 126, 1734–1744.

Schaer, M., Cuadra, M.B., Tamarit, L., Lazeyras, F., Eliez, S., Thiran, J.P., 2008. A surface-based approach to quantify local cortical gyrification. IEEE Trans. Med. Imaging 27, 161–170.

Scott, M.L., Thacker, N.A., 2005. Robust tissue boundary detection for cerebral cortical thickness estimation. Med. Image Comput. Comput. Assist. Interv. Int. Conf. Med. Image Comput. Comput. Assist. Interv. 8, 878–885.

Segonne, F., Pacheco, J., Fischl, B., 2007. Geometrically accurate topology-correction of cortical surfaces using nonseparating loops. IEEE Trans. Med. Imaging 26, 518–529.

Shattuck, D.W., Leahy, R.M., 2001. Automated graph-based analysis and correction of cortical volume topology. IEEE Trans. Med. Imaging 20, 1167–1177.

Sowell, E.R., Thompson, P.M., Leonard, C.M., Welcome, S.E., Kan, E., Toga, A.W., 2004. Longitudinal mapping of cortical thickness and brain growth in normal children. J. Neurosci. 24, 8223–8231.

Sowell, E.R., Peterson, B.S., Kan, E., Woods, R.P., Yoshii, J., Bansal, R., Xu, D., Zhu, H., Thompson, P.M., Toga, A.W., 2007. Sex differences in cortical thickness mapped in 176 healthy individuals between 7 and 87 years of age. Cereb. Cortex 17, 1550–1560.

Thompson, P.M., Hayashi, K.M., Sowell, E.R., Gogtay, N., Giedd, J.N., Rapoport, J.L., de Zubicaray, G.I., Janke, A.L., Rose, S.E., Semple, J., Doddrell, D.M., Wang, Y., van Erp, T.G., Cannon, T.D., Toga, A.W., 2004. Mapping cortical change in Alzheimer's disease, brain development, and schizophrenia. NeuroImage 23 (Suppl. 1), S2–S18.

Tohka, J., Zijdenbos, A., Evans, A., 2004. Fast and robust parameter estimation for statistical partial volume models in brain MRI. NeuroImage 23, 84–97.

Toro, R., Perron, M., Pike, B., Richer, L., Veillette, S., Pausova, Z., Paus, T., 2008. Brain size and folding of the human cerebral cortex. Cereb. Cortex. Q13

Tosun, D., Rettmann, M.E., Han, X., Tao, X., Xu, C., Resnick, S.M., Pham, D.L., Prince, J.L., 2004. Cortical surface segmentation and mapping. NeuroImage 23 (Suppl. 1), S108–S118.

Van Essen, D.C., Drury, H.A., 1997. Structural and functional analyses of human cerebral cortex using a surface-based atlas. J. Neurosci. 17, 7079–7102.

Van Essen, D.C., Drury, H.A., Dickson, J., Harwell, J., Hanlon, D., Anderson, C.H., 2001. An integrated software suite for surface-based analyses of cerebral cortex. J. Am. Med. Inform. Assoc. 8, 443–459.

Wu, Y., Warfield, S.K., Tan, I.L., Wells III, W.M., Meier, D.S., van Schijndel, R.A., Barkhof, F., Guttmann, C.R., 2006. Automated segmentation of multiple sclerosis lesion subtypes with multichannel MRI. NeuroImage 32, 1205–1215.

Xu, C., Pham, D.L., Rettmann, M.E., Yu, D.N., Prince, J.L., 1999. Reconstruction of the human cerebral cortex from magnetic resonance images. IEEE Trans. Med. Imaging 18, 467–480.

Yezzi Jr., A.J., Prince, J.L., 2003. An Eulerian PDE approach for computing tissue thickness. IEEE Trans. Med. Imaging 22, 1332–1339.

Yotter, R.A., Dahnke, R., Gaser, C., 2009. Topological correction of brain surface meshes using spherical harmonics. Med. Image Comput. Comput. Assist. Interv. 12, 125–132.

Yotter, R.A., Dahnke, R., Gaser, C., in press. Topological Correction of Brain Surface Meshes Using Spherical Harmonics. Hum. Brain Mapp. Q14

Zeng, X., Staib, L.H., Schultz, R.T., Duncan, J.S., 1999. Segmentation and measurement of the cortex from 3-D MR images using coupled-surfaces propagation. IEEE Trans. Med. Imaging 18, 927–937.

Zhang, K., Sejnowski, T.J., 2000. A universal scaling law between gray matter and white matter of cerebral cortex. Proc. Natl. Acad. Sci. U. S. A. 97, 5621–5626.

Zhang, Y., Brady, M., Smith, S., 2001. Segmentation of brain MR images through a hidden Markov random field model and the expectation-maximization algorithm. IEEE Trans. Med. Imaging 20, 45–57.

Please cite this article as: Dahnke, R., et al., Cortical thickness and central surface estimation, NeuroImage (2012), http://dx.doi.org/10.1016/j.neuroimage.2012.09.050